Transient electron precipitation during oscillatory BBF braking: THEMIS observations and theoretical estimates

E. V. Panov,[1] A. V. Artemyev,[2,3] W. Baumjohann,[1] R. Nakamura,[1] and V. Angelopoulos[4]

Received 2 November 2012; revised 21 February 2013; accepted 23 February 2013; published 11 June 2013.

[1] We use Time History of Events and Macroscale Interactions during Substorms (THEMIS) data acquired on 17 March 2008 between 10:22 and 10:32 UT to study the mechanism of transient electron injection into the loss cone during oscillatory bursty bulk flow (BBF) braking. During braking, transient regions of piled-up magnetic fluxes are formed. Perpendicular electron anisotropy observed in these regions (presumably caused by betatron perpendicular electron heating) may be a free-energy source of coexisting whistler waves. Parallel electrons with energies between 1 and 5 keV disappear inside these regions, and transient auroral forms (both rather discrete arcs and diffuse-like aurora around the arcs) are observed simultaneously by the ground all-sky imager at Fort Yukon. We use quasi-linear theory of electron resonant interaction with whistler waves and also estimate the effectiveness of electron nonlinear capture by strong whistler waves. We suggest that electron injection into the loss cone is caused by: (1) scattering by whistler waves and (2) parallel acceleration of electrons captured by stronger whistler waves.

Citation: Panov, E. V., A. V. Artemyev, W. Baumjohann, R. Nakamura, and V. Angelopoulos (2013), Transient electron precipitation during oscillatory BBF braking: THEMIS observations and theoretical estimates, *J. Geophys. Res. Space Physics*, *118*, 3065–3076, doi:10.1002/jgra.50203.

1. Introduction

[2] Night-side auroral forms are believed to be the ionospheric counterpart of substorm-associated phenomena in the plasma sheet [see, e.g., *Paschmann et al.*, 2002]. One such phenomenon is bursty bulk flows (BBFs), intermittent fast plasma flows inside the plasma sheet [*Hayakawa et al.*, 1982; *Baumjohann et al.*, 1989, 1990, 1991, 1999a; *Angelopoulos et al.*, 1992, 1994] that are believed to provide magnetic flux transport to overcome the "pressure balance inconsistency" [*Erickson and Wolf*, 1980; *Pontius and Wolf*, 1990; *Baumjohann*, 2002].

[3] Numerous reports suggest that auroral forms occur near the footprints of the magnetic field lines connected to BBFs [*Nakamura et al.*, 1993; *Elphinstone et al.*, 1995; *Henderson et al.*, 1998; *Lyons et al.*, 1999, 2011; *Sergeev et al.*, 2000, 2001; *Nakamura et al.*, 2001a, 2001b; *Amm and Kauristie*, 2002; *Borodkova et al.*, 2002; *Zesta et al.*, 2002; *Sergeev et al.*, 2004; *Kepko et al.*, 2004, 2009; *Keiling et al.*, 2009a, 2009b; *Frey et al.*, 2010; *Panov et al.*, 2010a; *Lui et al.*, 2010]. Some of these auroral forms, referred to as "auroral streamers" [e.g., *Elphinstone et al.*, 1996; *Sergeev et al.*, 1999; *Nakamura et al.*, 2001b], are thought to appear in type I current wedges [*Boström*, 1964; *Untiedt and Baumjohann*, 1993; *Birn and Hesse*, 2005], where forces perpendicular to the long axis of the generator plasma drive the generator current along the axis [see *Haerendel*, 2010 and references therein].

[4] Multispacecraft observations have revealed that BBFs occur in very localized channels only 2–3 R_E wide [*Angelopoulos et al.*, 1996; *Sergeev et al.*, 1996; *Nakamura et al.*, 2004]. At around $X \sim -10R_E$, they are suddenly decelerated by the dominant dipolar magnetic field, and pressure gradients pile up, leading to a substorm current wedge [*Haerendel*, 1992; *Shiokawa et al.*, 1997, 1998a, 1998b; *Baumjohann*, 2002; *Birn et al.*, 1999, 2004; *Ohtani et al.*, 2009] and substorm onset. As BBFs decelerate, they may overshoot and oscillate around an equilibrium position [*Semenov and Lebedeva*, 1991; *Chen and Wolf*, 1999; *Panov et al.*, 2010b; *Birn et al.*, 2011; *Wolf et al.*, 2012a, 2012b]. This oscillatory braking creates a partial alternating current in the substorm current wedge [*Panov et al.*, 2013b].

[5] Here, we use Time History of Events and Macroscale Interactions during Substorms (THEMIS) probe P1 [*Angelopoulos*, 2008] burst-mode electron and high-resolution electromagnetic observations and quasi-linear and non-linear theoretical calculations to reveal the mechanism of electron injection into the loss cone on 17 March 2008 between 10:20 and 10:40 UT [*Panov et al.*, 2010b, 2013b] that may form aurora during oscillatory BBF braking. The magnetotail observations were provided by the

[1]Space Research Institute, Austrian Academy of Sciences, Graz, Austria.
[2]Space Research Institute, Russian Academy of Sciences, Moscow, Russia.
[3]LPC2E/CNRS-University of Orleans, Orleans, France.
[4]Institute of Geophysics and Planetary Physics, University of California, Los Angeles, California, USA.

Corresponding author: E. V. Panov, Space Research Institute, Austrian Academy of Sciences, Schmiedlstraße 6, 8042 Graz, Austria. (evgeny_panov@mail.ru)

©2013. American Geophysical Union. All Rights Reserved.
2169-9380/13/10.1002/jgra.50203

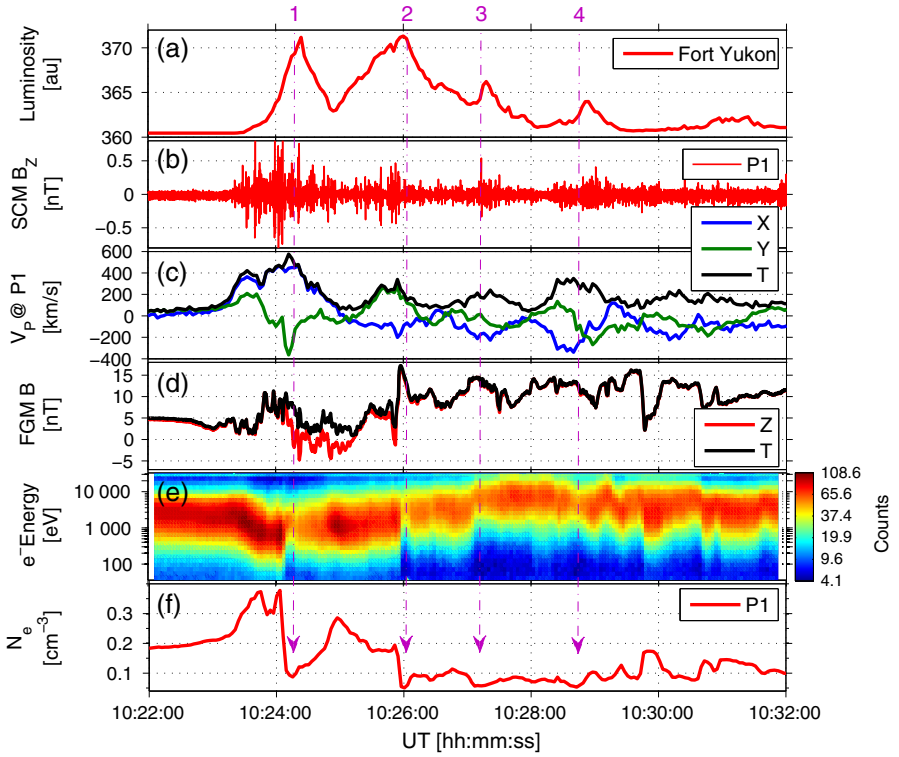

Figure 1. THEMIS data on 17 March 2008 between 10:22:00 and 10:32:00 UT: (a) total luminosity observed by the all-sky imager at Fort Yukon, (b) Z-component of the magnetic field oscillations from SCM, (c) X-, Y-, and total component of the ion velocity from ESA, (d) Z-, and total component of the magnetic field from FGM, (e) electron energy spectrogram, and (f) electron density from ESA at P1.

THEMIS FGM [*Auster et al.*, 2008], ESA [*McFadden et al.*, 2008], SCM [*Roux et al.*, 2008] instruments and ground-based observations provided by the all-sky imager (ASI) at Fort Yukon [*Mende et al.*, 2008].

2. THEMIS Observations

[6] THEMIS plasma sheet and ground observations between 10:22:00 and 10:32:00 UT on 17 March 2008 are presented in Figure 1. As shown by *Panov et al.* [2013b], the all-sky imager at Fort Yukon observed four separately evolving auroral forms accompanied by a substantial increase in the total luminosity (Figure 1a). The four auroral forms were detected during the first two periods of oscillatory BBF braking. Auroral forms 1 and 3 appeared to be related to the two earthward flows; auroral forms 2 and 4 appeared to be related to the two tailward recoils. *Panov et al.* [2013b] also pointed out that the four forms evolved as the upward alternating ionospheric field-aligned current appeared. At P1, which was located very close to the neutral sheet (total magnetic field almost equal to B_Z, Figure 1d), we observe electromagnetic wave activity (Figure 1b) correlated with four enhancements in auroral brightness (Figure 1a). There is always a discrepancy between timing of ground observations and timing observations in the plasma sheet. According to *Panov et al.* [2013b], the time delay between the ground and plasma sheet observations considered here is on the order of tens of seconds, considerably shorter than the flow oscillation period of about 2.5 min. Enhancements in the electromagnetic oscillation amplitude coincided with the faster plasma flows (Figure 1c), with the enhancements in the magnetic field (Figure 1d), and with the electron density decreases (Figures 1e and 1f); indicated by the four numbered magenta dashed vertical arrows.

2.1. Electrons

[7] As shown in Figure 1, the first and most significant earthward flow burst demonstrated the clearest magnetic field and plasma behavior during oscillatory BBF braking. In addition, the observations of the first auroral form at Fort Yukon showed the sharpest and brightest signatures [*Panov et al.*, 2013b]. We therefore use THEMIS observations during the first earthward flow burst. Figure 2a shows the electron energy distribution function on 17 March 2008 during the first earthward flow burst, both before (at 10:23:30 UT and 10:24:00 UT) and inside the magnetic field pile-up region with an electron density dip at 10:24:15 UT. One can see from Figure 2a that, inside the density dip at 10:24:15 UT, the lower-energy part of the electron population with energies between about 1 and 5 keV is missing. Figure 2b shows the pitch-angle electron distribution function for the same times. From this figure, one can see that the missing part of the electron population has parallel and anti-parallel pitch angles. Figure 2c shows the electron energy distribution function for quasi-parallel (pitch angle fewer than 15°) and quasi-perpendicular (pitch angle between 75° and 105°) electrons at 10:24:15 UT. The electrons inside the electron density dip have significant perpendicular temperature anisotropy. Such anisotropy is known to be a free energy source of whistler waves.

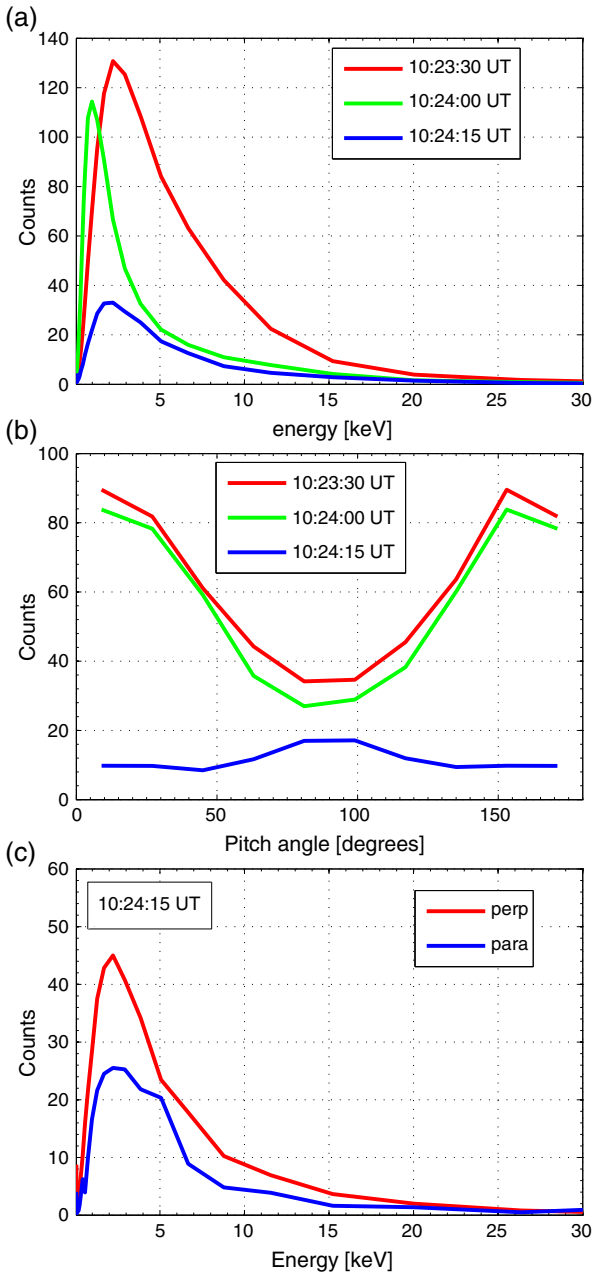

Figure 2. (a) Electron energy distribution function, (b) electron pitch-angle distribution function, and (c) electron energy distribution function for parallel (pitch-angle fewer than 15°) and perpendicular (pitch-angle between 75° and 105°) electrons on 17 March 2008 at and before 10:24:15 UT.

2.2. Whistler Waves

[8] Figure 3 shows EFI and SCM onboard, digitally computed filter bank spectra (FBK) of one electric field (top) and one magnetic field (bottom) component on 17 March 2008 between 10:22:00 and 10:32:00 UT. The maxima in the oscillation power around 10:24:15 UT and 10:26:00 UT correspond to auroral forms 1 and 2, as indicated in Figure 1. The enhanced oscillation power was observed between the lower-hybrid frequency (about 5 Hz) up to 1 kHz. Figure 4 shows the amplitudes of the electric field (left) and magnetic field (right) FBK component on 17 March 2008 at 10:24:15 UT (during the first earthward flow burst). The electric field oscillation power is comparable to the magnetic field oscillation power (normalized by the local Alfvén speed V_A ~1000 km/s), suggesting that the oscillations are electromagnetic. Considering the above results and the electron observations in Figure 2, one can suggest that the observed electromagnetic oscillations may be due to whistler waves generated by perpendicular electron anisotropy.

[9] Taking advantage of the three-component measurements of the lower band of these oscillations (up to 128 Hz) by the SCM and EFI instruments onboard P1, we calculated the wave Poynting flux. Figure 5 shows the electric and magnetic field observations from SCM and EFI onboard P1 on 17 March 2008 between 10:24:07.5 and 10:24:22.5 UT: X-, Y-, and Z- DSL components of the magnetic field oscillations (Figure 5a) and X-, Y-, and Z- DSL components of the electric field oscillations in the 6–128 Hz range (Figure 5b). The Z-component of the electric field (red curve in Figure 5b) is contaminated with spurious quasi-periodical spikes, four times per spin, due to sphere shadowing by the spacecraft body that do not affect our results. Between about 10:24:14.0 and 10:24:15.5 UT, there are indeed enhanced electromagnetic oscillations (Figures 5c and 5d). The Poynting flux of these oscillations is directed mainly parallel to the magnetic field (Figures 5e and 5f).

[10] Figure 6a shows the total (red), parallel (green), and perpendicular (blue) components of the integral Poynting flux between 10:24:13.5 and 10:24:16.0 UT. The parallel flux always dominates: the angle between the Poynting vector, and the magnetic field is on average about 20° (Figure 6b). We calculated the integral Poynting flux for different frequency ranges (not shown here). At any frequency in the 5–64 Hz range ($64 = \frac{128}{2}$ is the Nyquest frequency for the EFI and SCM measurements), a wave packet is always propagating at fewer than 30° to the ambient magnetic field between 10:24:14.0 UT and 10:24:15.5 UT. In addition, Figure 6c shows the polarization spectrogram that was calculated using perpendicular magnetic field components [see, e.g., *Baumjohann et al.*, 1999b, 2000]. There, bluish colors represent right-handed polarization of the electromagnetic oscillations. The electromagnetic oscillations at power peaks 1 and 2 are mainly right-hand polarized. The above facts suggest that the observed electromagnetic oscillations are whistler waves.

3. Theoretical Model of Electron Injection Into the Loss Cone

[11] Near the neutral plane (where $B_x \sim 0$), an unstable anisotropic electron population with $T_{e\perp}/T_{e\parallel} > 1$ generates whistler waves through the mechanism considered by *Vedenov and Sagdeev* [1961]. Such waves, which propagate obliquely to the magnetic field, are observed onboard spacecraft as intensification of high-frequency electromagnetic activity. Because the ratio of the plasma frequency to the electron gyrofrequency is about $\omega_{pe}/\Omega_e \approx 5$ and magnetic field pressure is much higher than electron pressure, we use a simplified dispersion relation for whistler waves, $\omega = \Omega_e \cos\theta/(1 + (\omega_{pe}/kc)^2)$, where θ is the angle between the wave-normal direction and the magnetic field [*Ginzburg and Rukhadze*, 1975]. We neglect the influence of thermal

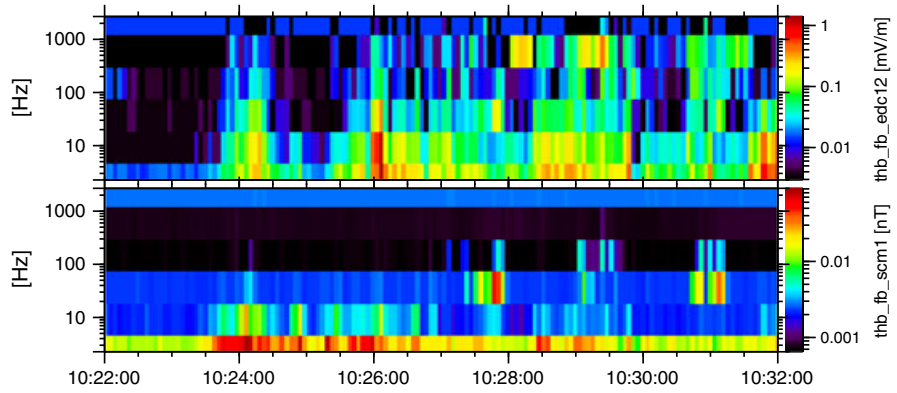

Figure 3. Onboard P1 filter bank spectra (FBK) of (top) one electric and (bottom) one magnetic field component on 17 March 2008 between 10:22:00 and 10:32:00 UT.

ions, assuming that $\omega/\Omega_i \gg 1$, where Ω_i is the ion gyrofrequency. This dispersion is valid when ω is substantially larger than the lower-hybrid frequency. Using the above THEMIS observations, we assume that $\omega/2\pi \sim 10 - 100$ Hz; the lower-hybrid frequency is $\sim 0.02(\Omega_e/2\pi) \sim 5$ Hz. The amplitude of the observed whistler waves is between 1 and 30 pT.

[12] The resonant interaction between whistler waves and electrons can provide effective electron scattering [*Trakhtengerts*, 1966; *Kennel and Petschek*, 1966]. Such scattering can be described as pitch-angle α diffusion; the scattering rate corresponds to the diffusion coefficient $D_{\alpha\alpha}$ [e.g., *Lyons*, 1974; *Glauert and Horne*, 2005 and references therein]. The resonant interaction between electrons and whistler waves results in electron scattering into the loss cone and electron precipitation. Below, we estimate the effectiveness of pitch-angle diffusion for the considered event.

[13] In addition to the quasi-linear theory of the wave-particle interaction corresponding to the broad wave spectrum, a nonlinear effect of particle capture by the observed strong whistler waves is also expected [*Solovev and Shkliar*, 1986; *Shklyar and Matsumoto*, 2009; *Bortnik et al.*, 2008]. The electrostatic part of whistler waves propagating at some nonzero angle θ provides a parallel electric field $E_\parallel$. If captured into the minima of the corresponding scalar potential, electrons would move with the wave in Landau resonance. Such motion in an inhomogeneous magnetic field results in energy gain by captured particles [see *Solovev and Shkliar*, 1986 and references therein]. Acceleration by Landau resonance leads to an increase in parallel velocity without a change in the perpendicular invariant—the magnetic moment. As a result, pitch-angle α effectively decreases in the neutral plane and particles may reach the loss cone. We observed several bursts of wave intensity with amplitudes around 1–3 mV/m. Because such waves can capture electrons, we describe the mechanism of capture below.

[14] We consider the geometry of the magnetic field corresponding to a dipolarized current sheet, i.e., $\mathbf{B} \approx B_0(z/L)\mathbf{e}_x + B_z\mathbf{e}_z$, where L is a spatial scale of B_x variation. Because of dipolarization, the amplitude of $B_x = B_0(z/L)$ is about $B_0 \approx B_z$. The lobe magnetic field should be around $\sim 3B_0$. We also introduce magnetic field magnitude such as $B(s) = \sqrt{B_x^2 + B_z^2} \approx B_0\sqrt{1 + (s/L)^2}$, where s is a coordinate along the field line.

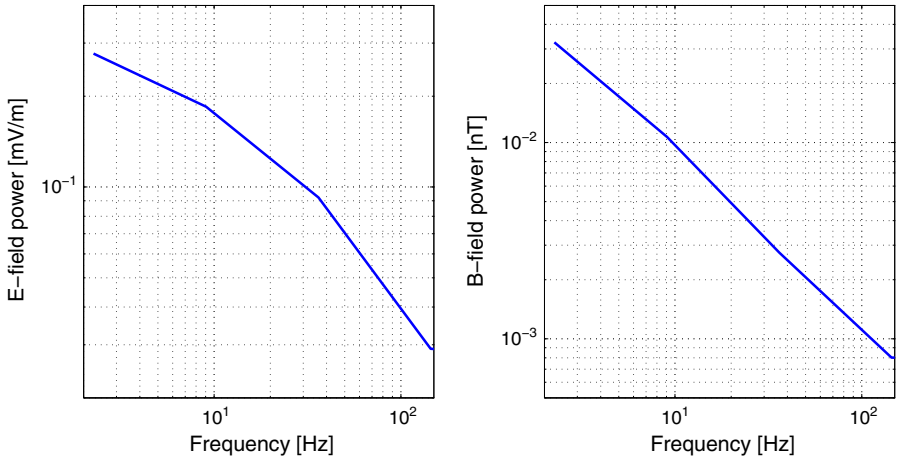

Figure 4. Onboard P1 FBK spectra of (left) the electric and (right) the magnetic field component shown in Figure 3 from 17 March 2008 at 10:24:15 UT.

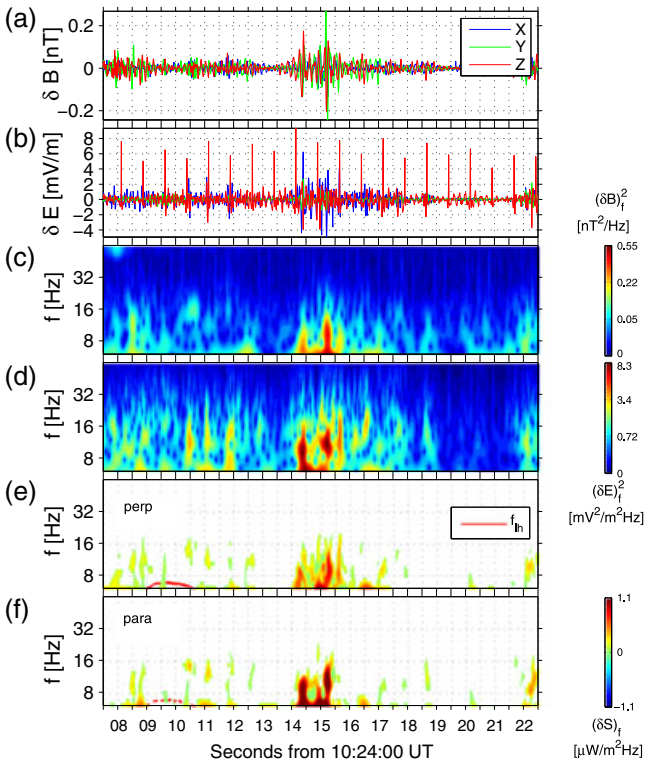

Figure 5. Electric and magnetic field observations from SCM and EFI onboard P1 on 17 March 2008 between 10:24:07.500 and 10:24:22.500 UT: (a) X-, Y-, and Z- DSL components of the magnetic field oscillations, (b) X-, Y-, and Z- DSL components of the electric field oscillations in the 6–128 Hz range, (c) wavelet spectrum of the Y_{DSL} component of the magnetic field oscillations, (d) wavelet spectrum of the X_{DSL} component of the electric field oscillations, (e) perpendicular and (f) parallel components of the Poynting flux.

3.1. Scattering by Whistler Waves

[15] If the resonant condition $\omega - k\cos\theta v_{\|} = n\Omega_e$ (where $v_{\|}$ is the parallel electron velocity and $\Omega = |e|B_0/m_e c$ is the electron gyrofrequency) is satisfied, waves can interact effectively with electrons. The combination of the resonant condition and the dispersion relation gives resonant frequency $\omega_{i,n}$ and the corresponding resonant wave number $k_{i,n}$ as functions of θ and $v_{\|}$ (n is the harmonic number and i is the resonance root number for a given n).

[16] To describe electron scattering caused by pitch-angle diffusion corresponding to the resonant interaction with whistler waves, we calculate the diffusion coefficient $D_{\alpha\alpha}$ following the approach proposed by *Glauert and Horne* [2005]:

$$D_{\alpha\alpha} = \frac{e^2}{4\pi}\sum_{i,n}\int_{X_{\min}}^{X_{\max}} \frac{G\hat{B}^2|\Phi_n|^2 X\mathrm{d}X}{1+X^2}\frac{|n\Omega_e - \omega_{i,n}\sin^2\alpha|^2}{\cos^2\alpha|v_{\|} - \frac{\partial\omega}{\partial k_{\|}}|} \quad (1)$$

where we introduce a new variable of integration $X = \tan\theta$ and write a nonrelativistic expression for $D_{\alpha\alpha}$. The term $|\Phi_n|^2$ corresponds to the relation between different components of wave's electromagnetic field [*Lyons*, 1974; *Glauert and Horne*, 2005]. Function $\hat{B}^2(\omega_{i,n})$ determines the distribution of wave power density over frequency. In this paper, we made two runs of calculations with different $\hat{B}^2$. The first run corresponds to a power law spectrum (as shown in Figure 4):

$$\hat{B}^2(\omega) = A(\omega/\delta\omega)^{-h_\omega},\ \omega \in [\omega_-, \omega_+] \quad (2)$$

and $\hat{B}^2 = 0$ if $\omega \notin [\omega_-, \omega_+]$, where $\omega_-/2\pi = 10$Hz, $\omega_+/2\pi = 1000$Hz, $\delta\omega = \omega_-$, and $h_\omega = 2$.

[17] The resolution of the observed spectrum is relatively rough, however, and we could miss some local maximum (if any) of $\hat{B}^2(\omega)$. To check the role of such a maximum, we use the second run with

$$\hat{B}^2(\omega) = A\exp\left(-\left(\frac{\omega-\omega_m}{\delta\omega}\right)^2\right),\ \omega \in [\omega_-, \omega_+] \quad (3)$$

and $\hat{B}^2 = 0$ if $\omega \notin [\omega_-, \omega_+]$, where $\omega_\pm = \omega_m \pm \Delta\omega$. We take $\omega_m = 0.35\Omega_e$, $\delta\omega = 0.15\Omega_e$ and $\Delta\omega = 1.5\delta\omega$ [typical parameters for whistler wave activity observed in radiation belts, see, e.g., *Glauert and Horne*, 2005]. For both runs, the constant A is obtained from the normalization $\int_{\omega_-}^{\omega_+}\hat{B}^2(\omega)\mathrm{d}\omega = B_w^2$, where B_w is the wave mean amplitude.

[18] Function $G = G(X)$, which corresponds to wave distribution over θ angle and can be defined as [see details in *Lyons*, 1974; *Glauert and Horne*, 2005]:

$$G(X) = 2\pi^2 g(X)/\int_{X_{\min}}^{X_{\max}}\frac{g(X)X}{(1+X^2)^{3/2}}k_{i,n}^2\left.\frac{\partial k}{\partial\omega}\right|_X \mathrm{d}X$$

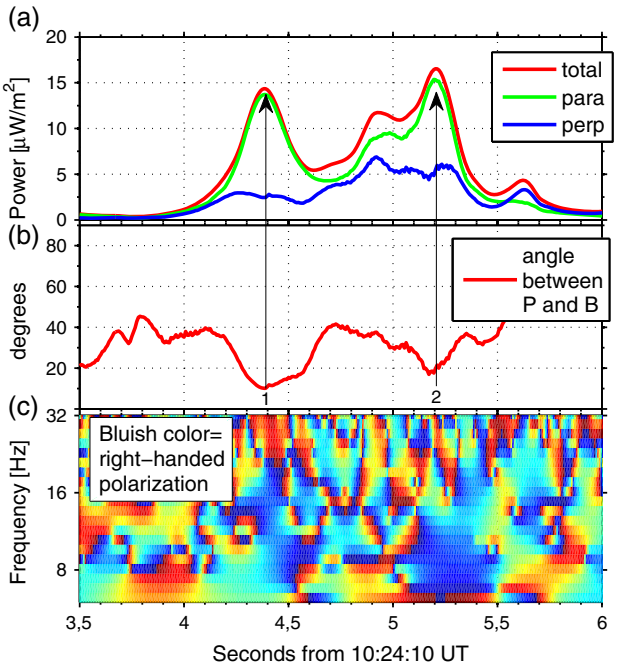

Figure 6. (a) Total (red), parallel (green), and perpendicular (blue) components of the integral Poynting flux; (b) angle between the integral Poynting flux and the magnetic field direction for the electromagnetic oscillations from SCM and EFI instruments onboard P1; and (c) polarization spectrogram with bluish colors representing right-handed polarization on 17 March 2008 between 10:24:13.500 and 10:24:16.000 UT.

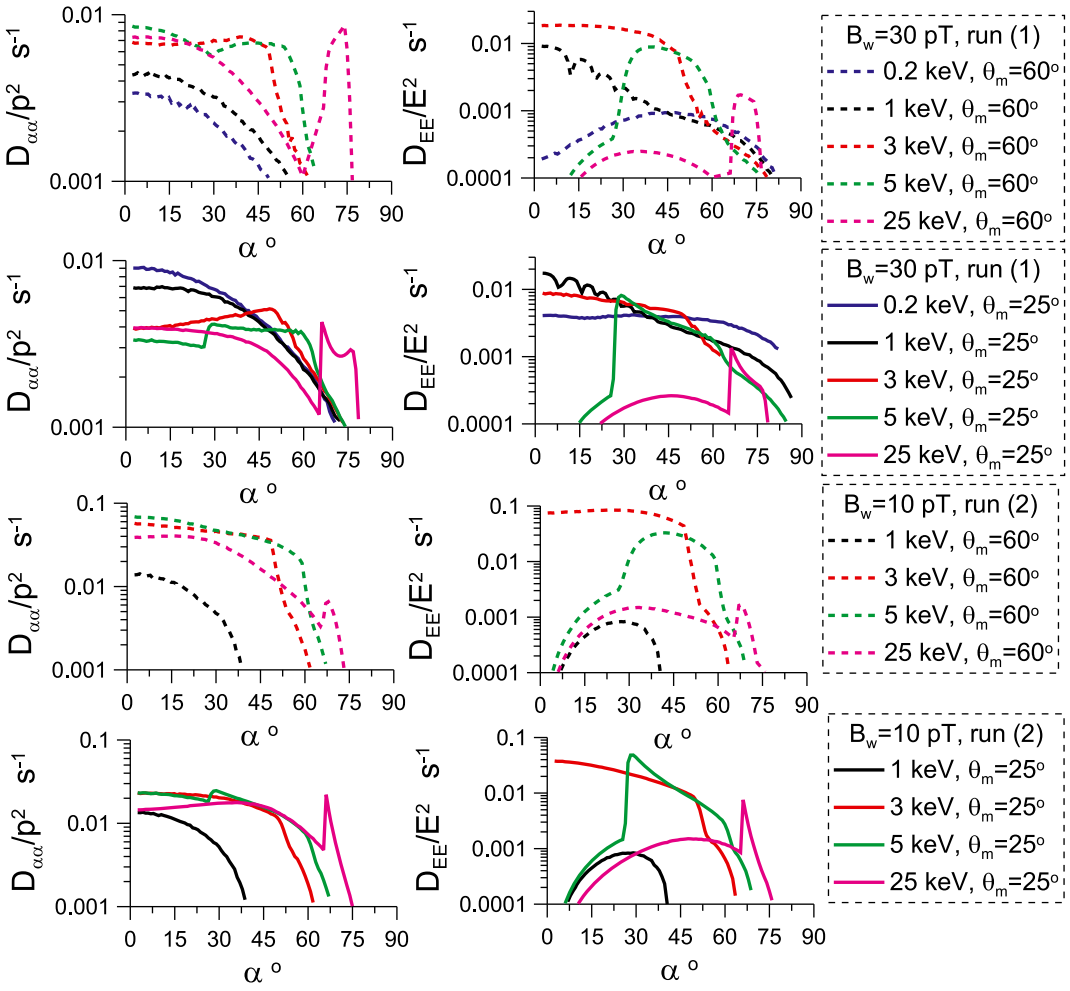

Figure 7. Normalized pitch-angle and energy diffusion coefficients as functions of electron pitch-angle α for different energies and mean angles of wave propagation θ_m. Here, p is the electron total momentum and E is the electron energy.

where $g(X) = \exp(-(X-X_m)^2/X_w^2)$ with mean value $X_m = \tan\theta_m$ and variance X_w. Here, we use variance $X_w = 0.577$ (the corresponding angle dispersion would be about 30°).

[19] Figure 7 shows the calculated diffusion coefficients $D_{\alpha\alpha}$ for several energies and two values of θ_m, 25° and 60°. Here, we use the local values of $D_{\alpha\alpha}$ that are calculated for the neutral plane ($B_x = 0$). Bounce-averaging may somewhat modify the obtained results [e.g., for dipole magnetic field averaging over electron bounce oscillations results in a fivefold decrease in the magnitude of $D_{\alpha\alpha}$, see *Glauert and Horne*, 2005]. If we take into account background magnetic field differences and the effect of bounce averaging, our results shown in Figure 7 would coincide with the pitch-angle diffusion rates of low energy electrons in radiation belts [*Ni et al.*, 2011b].

[20] In the two distributions of $\hat{B}^2(\omega)$, $D_{\alpha\alpha}$ has similar amplitudes. However, it is slightly larger for the distribution with a localized peak (equation 3), where the spectral density at $\omega \sim 0.35\Omega_e$ appears to be around 10 pT (see Figure 7, second run). On the other hand, the absence of waves in a small-frequency range results in the absence of resonant conditions for low-energy electrons: there is no scattering of 0.2 keV electrons in the second run. θ_m increase produces two effects: for low-energy electrons $D_{\alpha\alpha}$ decreases, and for electrons with energy near 3 keV $D_{\alpha\alpha}$ increases (Figure 7, first run). The increase in $D_{\alpha\alpha}$ with θ_m corresponds to a shift in the resonance condition to smaller pitch angles [see *Mourenas et al.*, 2012b]. Note that the maximum diffusion coefficient $D_{\alpha\alpha}$ corresponds to the energy range between 1 and 5 keV. Indeed, this electron population has a smaller parallel-to-perpendicular flux ratio (see Figure 2). Therefore, we suggest that the decrease in the parallel electron fluxes caused not only by betatron heating but also by scattering of electrons with small pitch angles due to diffusion.

[21] One can see in Figure 8 that the main contribution to the pitch-angle diffusion corresponds to the first cyclotron resonance $n = -1$ and Landau resonance $n = 0$. Here, we show $D_{\alpha\alpha}$ that was calculated for $n = \pm1, 0, -2$. For $n = 0$, the resonance condition $v_{||} = \omega/k\cos\theta$ can be satisfied only for electron energies larger than a certain threshold ($> (\omega/k\cos\theta)^2 m_e/2$). The main impact from this resonance can be found for intermediate pitch angles. The first cyclotron resonance $\omega = k\cos\theta v_{||} - \Omega_e$, which can be important even for very small $\omega \ll \Omega_e$ and contributes mainly to pitch-angle scattering of electrons with smaller pitch angles. The

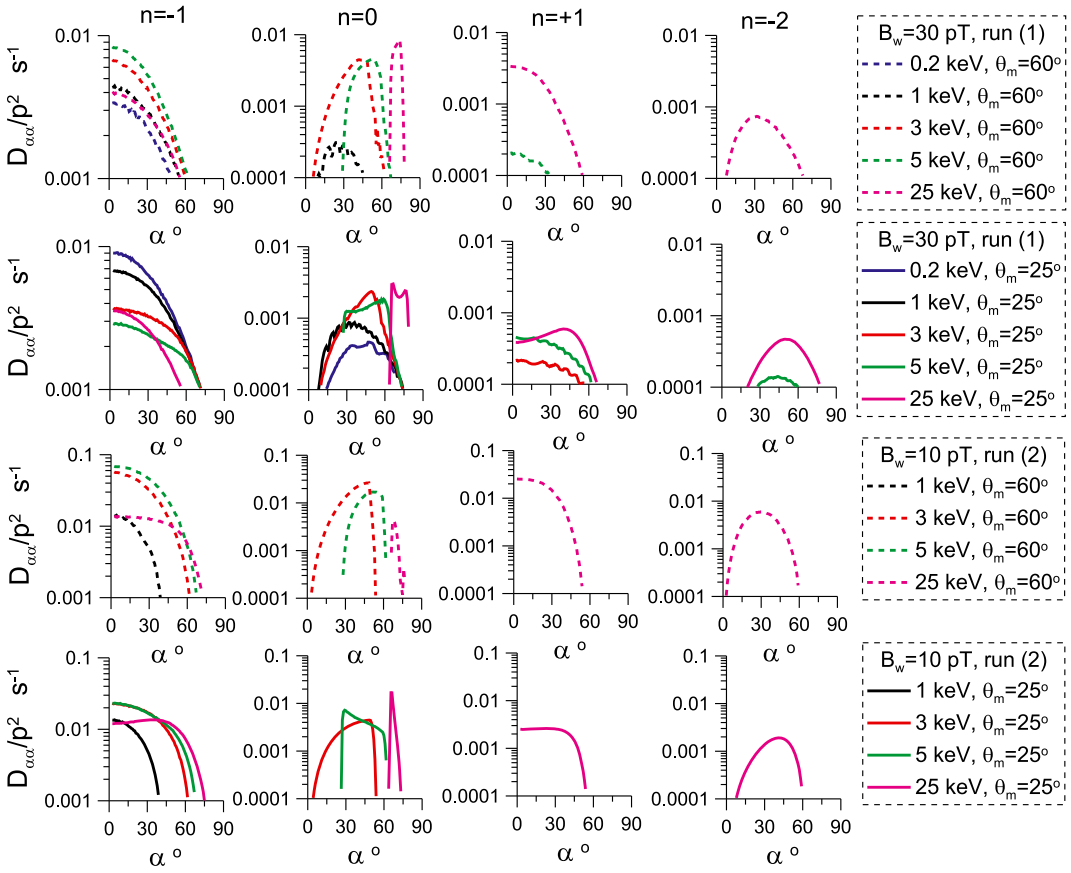

Figure 8. Normalized pitch-angle partial diffusion coefficients for $n = \pm 1, 0, -2$ as functions of electron pitch-angle α for different energies and mean angles of wave propagation θ_m.

resonances with larger cyclotron harmonics $n = 1, -2$ are important only for high-energy electrons.

[22] For the system considered, the loss-cone pitch angle can be estimated as $\alpha_{LC} \sim \sqrt{B_z/B^*} \sim 0.5°$ with the ionospheric magnetic field $B^* \sim 55$ μT. Note that α_{LC} increases substantially due to growing B_z. In the vicinity of the loss-cone, the pitch-angle diffusion rate is on the order of $D_{\alpha\alpha} \sim 10^{-2} - 10^{-3}$ s^{-1}. The corresponding timescale of electron scattering into the loss cone can be estimated as $\int D^{-1}_{\alpha\alpha} \tan^{-1}\alpha d\alpha \sim D^{-1}_{\alpha\alpha} \ln(\sin\bar{\alpha}/\sin\alpha_{LC}) \sim 100$ s, where $\bar{\alpha} \sim 30°$ is the upper boundary of the considered electron population [*Albert and Shprits*, 2009]. Then after about 1–2 minutes, a substantial part of the electron population should be scattered into the loss cone. This time is comparable to the time interval during which the dipolarization front would travel from mid-magnetotail into the near-Earth region. Therefore, we conclude that in the course of their earthward motion, electrons have sufficient time to be scattered into the loss cone.

[23] With the help of quasi-liner theory, the rates of energy diffusion D_{EE}, where E is the nonrelativistic electron energy [see *Glauert and Horne*, 2005], can be calculated:

$$D_{EE} = \frac{e^2}{4\pi}\frac{2E}{m_e}\sum_{i,n}\int_{X_{min}}^{X_{max}} \frac{G\hat{B}^2|\Phi_n|^2 X dX}{1+X^2}\frac{\omega_{i,n}^2 \sin^2\alpha}{|v_\parallel - \frac{\partial\omega}{\partial k_\parallel}|}$$

These coefficients define the rates of particle energization due to resonant interaction with whistler waves. The absence of $n\Omega_e - \omega_{i,n}\sin^2\alpha$ in the expression for D_{EE} results in a larger increase in D_{EE} than in $D_{\alpha\alpha}$ (see Figure 7). This effect is substantial for the system where only the first cyclotron resonance $n = -1$ and Landau resonance $n = 0$ play significant roles. For higher-energy electrons with $E > 10$ keV, the input of the higher order resonances (with $|n| > 1$) into the scattering leads to $D_{\alpha\alpha}$ larger than D_{EE} [see *Glauert and Horne*, 2005]. The time required for electron energization is comparable to or less than the time for scattering. As a result, a part of the electron population with energies between 1 and 5 keV may gain energy before scattering into the loss cone. Moreover, the electrons scattered into the loss-cone decelerate due to the energy diffusion and increase the intensity of whistler waves [see *Summers et al.*, 1998; *Mourenas et al.*, 2012a].

[24] Both mechanisms—electron scattering and energy diffusion—result in decreasing electron parallel fluxes in the energy range 1 – 5 keV. This conclusion agrees with the observations shown in Figure 2.

3.2. Resonant Capture by Whistler Waves

[25] In addition to the wide spectrum of whistler waves with an average magnetic field oscillation amplitude of about 1 – 10 pT and an electric field oscillation amplitude of about < 1 mV/m, we also observe sporadic bursts of the electric field with the larger (~ 1–3 mV/m) amplitudes. These bursts

show signatures of strong whistler waves recently found in the radiation belts [e.g., *Cattell et al.*, 2008]. Because of the relatively weak background magnetic field $B_z \approx 10$ nT and a weak gradient $\partial B/\partial s$, such waves may also effectively interact with electrons in a nonlinear regime. We consider the effects of such interaction. We start with guiding-center equations of motion for nonrelativistic electrons in an inhomogeneous magnetic field $B(s)$ and an electrostatic wave field $E_\parallel = E_0 \cos\phi$, where $\phi = k_\parallel s - \omega t$ [see details in *Solovev and Shkliar*, 1986]:

$$m_e \ddot{s} = -\mu \frac{\partial B}{\partial s} - eE_0 \cos\phi \qquad (4)$$

Here, $\dot{s} = v_\parallel$ and $\mu = m_e v_{\perp 0}^2/2B_0$ is the magnetic moment with perpendicular velocity in the neutral plane $v_{\perp 0}^2$. We neglect the effect of the perpendicular component of the electric field, assuming that the gyromotion is sufficiently fast to provide the conservation of μ for one electron bounce period. We also neglect any inhomogeneity in $k_\parallel$ along the field line [a more general theory can be found in *Solovev and Shkliar*, 1986; *Shklyar and Matsumoto*, 2009].

[26] In the vicinity of Landau resonance $\dot{\phi} = 0$, one can rewrite equation (4) as

$$\begin{cases} \ddot{\phi} = -\mathrm{A}(s) - \mathrm{B}(s)\sin\phi \\ \mathrm{A}(s) = \frac{k_\parallel \mu}{m_e}\frac{\partial B}{\partial s},\ \mathrm{B}(s) = \frac{k_\parallel eE_0}{m_e} \end{cases}$$

Because $\omega/k_\parallel$ is close to the electron thermal velocity (for 1 – 10 keV electrons) and ω is much larger than the bounce oscillation frequency $\sim \sqrt{\partial \mathrm{A}/\partial s}$, we introduce phase ϕ as a fast variable and s as a slow variable. We then write the Hamiltonian system with $H_\phi = (1/2)\dot{\phi}^2 + (\mathrm{A}(s)\phi + B(s)\cos\phi)$, a Hamiltonian of a nonlinear pendulum with a phase portrait shown in Figure 9a. If B > A, there are trapped (or captured) particles in the system (with closed trajectories and an average $\dot{\phi} = 0$ in Figure 9a). Here, we estimate parameter A in the vicinity of the neutral plane as $\mathrm{A} \approx k_\parallel v_{\perp 0}^2 s/2L^2$. Thus, we have $\mathrm{A/B} \approx (T_e/eLE_0)(s/L)$, where T_e is the electron temperature. For the $\omega/2\pi \sim 10 - 30$ Hz frequency range (i.e., $\omega/\Omega_e \sim 0.1$), the parallel electric field can be estimated from observations as $E_0 \sim 1 - 5$ mV/m. The corresponding ratio is $T_e/eLE_0 \sim 0.2 - 1$ for $L \sim 1000$ km and $T_e \sim 1$ keV. Therefore, in the vicinity of the neutral plane, B > A, and at $s/L \sim 3$, we have A > B. Electrons can be captured by the wave near the neutral plane and escape from the resonance in $s/L \sim 3$. The corresponding energy gain is $\sim \mu \Delta B(s) \sim m_e v_{\perp 0}^2/2$. The maximum increase in the parallel velocity for one capture-escape event is about $\Delta v_\parallel \sim \sqrt{2\mu \Delta B(s)/m_e} \sim v_{\perp 0}$. A true increase in $v_\parallel$, however, may be smaller, because a part of the gained energy may be transferred to $v_\perp$.

[27] The particle trajectory obtained using the numerical solution of equation (4) is shown in Figures 9b and 9c. An electron initially oscillates between the mirror points (bounce oscillations) and then is captured by the wave. It gains energy from its motion along the increasing magnetic field with a constant parallel velocity $\sim \omega/k_\parallel$ as it is captured. Finally, the electron escapes from the resonance with an increased parallel energy (the distance between the neutral plane and the mirror points grows). To calculate this trajectory, we use the model magnetic field with a gradient

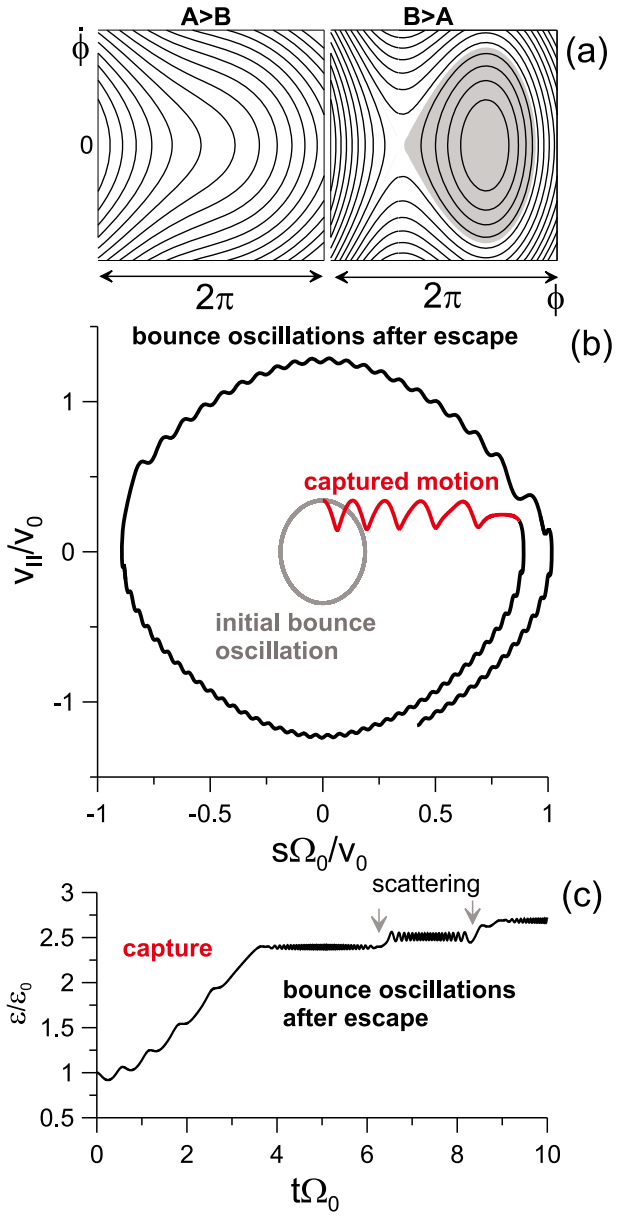

Figure 9. (a) Phase portraits for Hamiltonian system $H_\phi = (1/2)\dot{\phi}^2 + (\mathrm{A}(s)\phi + B(s)\cos\phi)$. Grey indicates region filled by trajectories of captured particles [see details in *Solovev and Shkliar*, 1986; *Artemyev et al.*, 2010]. (b) Particle trajectory in phase plane $(s, v_\parallel)$. Here, Ω_0 is the frequency of bounce oscillations, energy is $\varepsilon = m_e(v_\parallel^2 + v_\perp^2)/2$ and $\varepsilon_0 = m_e v_0^2/2$ is initial energy. Grey shows the trajectory before capture; red is used for the fragment corresponding to captured motion; and black shows the trajectory after escape. (c) Particle energy during captured motion and after escape.

$\partial B/\partial s = s/L^2$. In a real situation, $\partial B/\partial s \sim (s/L^2)/\sqrt{1 + (s/L)^2}$ and electrons may leave the current sheet because $\partial B/\partial s$ is finite. In such a case, calculation of new mirror points assumes a global magnetic field model of the magnetosphere that also includes slow growth of $B(s)$ towards the Earth.

[28] Additionally to the capture-escape phenomena, one can see in Figures 9b, and 9c small variations of particle energy that are due to the scattering of particles on the wave.

This effect is a consequence of the above described slow diffusion.

[29] We can also estimate the decrease in the electron pitch-angle $\Delta\alpha$ due to a single capture. We define $\tan\alpha = v_\perp/v_\parallel$ and write $\Delta\alpha \approx -\cos^2\alpha(v_\perp\Delta v_\parallel/v_\parallel^2) \approx \cos^2\alpha\tan^2\alpha = \sin^2\alpha$, where we take into account that $\Delta v_\parallel/v_\parallel = (v_\perp/v_\parallel)(\Delta v_\parallel/v_\perp) \approx \tan\alpha$ because $\Delta v_\parallel \approx v_\perp$. Hence, if we consider particles with $\sin\alpha \ll 1$, $|\Delta\alpha| \sim \alpha^2 \ll \alpha$. For electrons with $\alpha \sim 40° - 60°$, the change in the pitch-angle is $|\Delta\alpha| \sim 30° - 45°$ and the corresponding decrease in α becomes substantial. A similar effect of a decreasing electron pitch-angle due to the capture has been shown recently for strong whistler waves in radiation belts [*Artemyev et al.*, 2012] and also for EMIC waves [*Omura and Zhao*, 2012].

4. Discussion

[30] In the above analysis of THEMIS burst-mode electron and high-resolution electromagnetic wave observations on 17 March 2008 between 10:22 and 10:32 UT, we investigate the mechanism of electron injection into the loss cone that may form aurora [*Panov et al.*, 2013b] during oscillatory BBF braking [*Panov et al.*, 2010b].

[31] Based on the observed correlation between THEMIS space observations (electromagnetic wave activity and substantial escape of parallel electrons with energies between 1 and 5 keV) and ground observations (auroral luminosity at the footprints of geomagnetic field lines connected to the BBF), we find that the plasma sheet regions from which the electrons are injected into the loss-cone are magnetic flux pile-ups (usually referred to as dipolarization fronts). Most electron energization at dipolarization fronts appear to be perpendicular to the magnetic field, perhaps, due to betatron acceleration [for more details of this heating mechanism at dipolarization fronts, see *Fu et al.*, 2011; *Khotyaintsev et al.*, 2011].

[32] Earlier studies showed that whistler waves exist at dipolarization fronts [*Wei et al.*, 2007; *Le Contel et al.*, 2009; *Deng et al.*, 2010; *Huang et al.*, 2012; *Liang et al.*, 2012]. *Lyons et al.* [2012] present several THEMIS events in which dipolarization fronts occur simultaneously with auroral forms in conjugate ionospheric locations. Based on correlation between the plasma sheet THEMIS observations and the ground-based ASI observations at Fort Yukon, we find that the transient electron precipitation during oscillatory BBF braking may indeed originate from dipolarization fronts in the plasma sheet due to electron interaction with whistler waves.

[33] Our study further extends the recent results by *Thorne et al.* [2010] and *Ni et al.* [2011b] who showed that whistler-mode chorus waves are responsible for diffuse aurora, and also the one by *Nishimura et al.* [2010] who showed a correlation between whistler-mode waves and pulsating aurora. While previous results were obtained for whistler wave interaction with electrons in the inner magnetosphere, in our paper, we have shown that similar mechanisms can be responsible for electron precipitation from the magnetotail region.

[34] Based on the above observations, we calculate quasi-linear pitch-angle and energy diffusion coefficients, i.e., rates of electron scattering on the observed whistler waves. We also estimate the non-linear effects of resonant electron capture and consequent parallel acceleration by strong whistler waves near a dipolarization front. We find that both mechanisms may be equally efficient and seem to operate together. Specifically, we find that the considered diffusion would be especially effective for electrons with energies between 1 and 5 keV (in agreement with Figure 2c), which shows that most electrons missing at dipolarization fronts are parallel electrons that coexist with strong, nearly parallel-propagating whistler waves. The simultaneous disappearance of the plasma sheet electrons with energies between 1 and 5 keV at dipolarization fronts that were magnetically conjugate to the auroral forms' location in the ionosphere suggests that the missing parallel electrons and the precipitated electrons may be the same particles. Note that the all-sky camera observations at Fort Yukon [*Panov et al.*, 2013b] show the presence of both rather discrete arcs and diffuse-like aurora around the arcs. Because of errors in the footprint identification, we are, however, yet unable to claim which one of them is due to electron-whistler interactions. Note also that we are unable to measure the loss cone electrons directly because the time resolution of the particle detector is larger than the electron bounce time, and the pitch angle is less than few degrees.

[35] Here, we should mention, that Figure 3 demonstrates the presence of wave activity up to 1–2 kHz. These are mainly electrostatic fluctuations (compare top and bottom panels) with amplitudes around 0.1 mV/m. Thus, we probably observe electron cyclotron waves. Such waves can also scatter electrons into the loss cone [*Ni et al.*, 2011a] and form diffuse aurora [*Liang et al.*, 2011]. However, the amplitudes of the electric field fluctuations at $\sim$ 1 kHz are one to two orders of magnitude smaller than the corresponding amplitudes of the whistler waves around $\sim$ 100 Hz. Therefore, the whistler waves are supposed to play a more important role for electron scattering than the electron cyclotron waves.

[36] The electron-whistler interaction is probably limited to the plasma sheet around the neutral sheet plane, as observed by P1. The other THEMIS probes, which were closer to the plasma sheet boundary layer (B_x exceeded 15 nT), observed less clear wave-activity (not shown here).

[37] In addition to the above quasi-linear and non-linear electron-whistler interaction, some electrons may precipitate at dipolarization fronts directly through transient loss-cone widening that occurs because of the larger equatorial magnetic field B_z inside those dipolarization fronts. In the above observations, the loss-cone at the dipolarization fronts appeared to be about two times wider than the loss-cone in the ambient plasma (0.5°). Note that because of the absence of spacecraft observations in the low-altitude magnetosphere, we are unable to study the effects of parallel electric fields for auroral arc formation.

[38] Finally, it is interesting that according to our observations, the regions where the electrons reach the loss cone and precipitate moved past the spacecraft just few seconds. Taking into account the highest BBF velocity of about 500 km/s, one can come up with a scale of only few thousand kilometers in the plasma sheet. Such scales are in agreement with the ground all-sky imager observation of auroral form thicknesses on the order of tens of kilometers [see *Panov et al.*, 2013b for auroral images].

[39] Interesting to note that recently there were reported observations of a longitudinally propagating arc wave (LPAW) [*Uritsky et al.*, 2009; *Keiling et al.*, 2012]. For one of these observations, on 5 March 2008, between 5:50 and 6:05 UT *Panov et al.* [2012a] have shown that the plasma sheet exhibited signatures of a kinetic ballooning/interchange instability [*Pritchett and Coroniti*, 2010] before the substorm onset. This would be another example of quasi-periodical auroral brightening response to the plasma sheet activity.

5. Conclusions

[40] During oscillatory BBF braking on 17 March 2008 between 10:22 and 10:32 UT,

[41] 1. Regions of piled-up magnetic flux formed where the perpendicular electron anisotropy was observed, presumably due to betatron perpendicular electron heating.

[42] 2. We suggest that such anisotropy would explain the observed coexistence of whistler waves.

[43] 3. That parallel low-energy electrons lacked inside these regions, and auroral forms observed by ground all-sky imager in conjugate ionospheric location near Fort Yukon suggests that the lacking parallel plasma sheet electrons and the precipitated electrons may be the same particles. Note that because of errors in the spacecraft footprint identification and lack of spacecraft observations of parallel electric fields in the low-altitude magnetosphere, it is not clear whether the electron-whistler interactions caused discrete auroral arcs or diffuse-like aurora around the arcs.

[44] 4. According to the presented analytical calculations, we suggest that the electrons diffused into the loss-cone largely through: (1) scattering on the whistler waves and (2) parallel acceleration of the electrons trapped by the whistler waves. The most effective diffusion is predicted to be for the plasma sheet electrons with energies between 1 and 5 keV, in agreement with THEMIS observations.

[45] **Acknowledgments.** We acknowledge NASA contract NAS5-02099 for the use of data from the THEMIS Mission. Specifically: U. Auster and K.-H. Glaßmeier for the use of FGM data provided under the lead of the Technical University of Braunschweig and with financial support through the German Ministry for Economy and Technology and the German Center for Aviation and Space (DLR) under contract 50 OC 0302, J. W. Bonnell and F. S. Mozer for the use of EFI data, A. Roux and O. Le Contel for the use of SCM data, S. Mende and E. Donovan, and the CSA for logistical support in fielding and data retrieval from the GBO stations. The authors acknowledge J. Hohl for helping with editing. Work of A.V.A. was supported by grants of Leading Schools NIII-623.2012.2, and by the Program (OFN-15) of the Division of Physical Sciences of the Russian Academy of Sciences. The work was partly supported by the Austrian Science Fund (FWF) I429-N16, and by the Seventh Framework European Commission Programme (FP7, project 269198 - 'Geoplasmas').

References

Albert, J. M., and Y. Y. Shprits (2009), Estimates of lifetimes against pitch angle diffusion, *J. Atm. Solar-Terr. Phys.*, *71*, 1647–1652, doi:10.1016/j.jastp.2008.07.004.

Amm, O., and K. Kauristie (2002), Ionospheric Signatures Of Bursty Bulk Flows, *Surv. Geophys.*, *23*, 1–32, doi:10.1023/A:1014871323023.

Amm, O., R. Nakamura, T. Takada, K. Kauristie, H. U. Frey, C. J. Owen, A. Aikio, and R. Kuula (2011), Observations of an auroral streamer in a double oval configuration, *Ann. Geophys.*, *29*, 701–716, doi:10.5194/angeo-29-701-2011.

Angelopoulos, V. (2008), The THEMIS mission, *Space Sci. Rev.*, *141*, 5–34, doi:10.1007/s11214-008-9336-1.

Angelopoulos, V., W. Baumjohann, C. F. Kennel, F. V. Coronti, M. G. Kivelson, R. Pellat, R. J. Walker, H. Luehr, and G. Paschmann (1992), Bursty bulk flows in the inner central plasma sheet, *J. Geophys. Res.*, *97*, 4027–4039, doi:10.1029/91JA02701.

Angelopoulos, V. et al. (1994), Statistical characteristics of bursty bulk flow events, *J. Geophys. Res.*, *99*, 21,257–21,280, doi:10.1029/94JA01263.

Angelopoulos, V., et al. (1996), Multipoint analysis of a bursty bulk flow event on April 11, 1985, *J. Geophys. Res.*, *101*, 4967–4990, doi:10.1029/95JA02722.

Artemyev, A., V. Krasnoselskikh, O. Agapitov, D. Mourenas, and G. Rolland (2012), Non-diffusive resonant acceleration of electrons in the radiation belts, *Phys. Plasmas*, *19*, 122,901, doi:10.1063/1.4769726.

Artemyev, A. V., A. I. Neishtadt, L. M. Zelenyi, and D. L. Vainchtein (2010), Adiabatic description of capture into resonance and surfatron acceleration of charged particles by electromagnetic waves, *Chaos*, *20*(4), 43–128, doi:10.1063/1.3518360.

Auster, H. U., et al. (2008), The THEMIS fluxgate magnetometer, *Space Sci. Rev.*, *141*, 235–264, doi:10.1007/s11214-008-9365-9.

Baumjohann, W. (2002), Modes of convection in the magnetotail, *Phys. Plasmas*, *9*, 3665–3667, doi:10.1063/1.1499116.

Baumjohann, W., G. Paschmann, and C. A. Cattell (1989), Average plasma properties in the central plasma sheet, *J. Geophys. Res.*, *94*, 6597–6606, doi:10.1029/JA094iA06p06597.

Baumjohann, W., G. Paschmann, and H. Luehr (1990), Characteristics of high-speed ion flows in the plasma sheet, *J. Geophys. Res.*, *95*, 3801–3809, doi:10.1029/JA095iA04p03801.

Baumjohann, W., G. Paschmann, T. Hagai, and H. Luehr (1991), Superposed epoch analysis of the substorm plasma sheet, *J. Geophys. Res.*, *96*, 11,605–11,608, doi:10.1029/91JA00775.

Baumjohann, W., M. Hesse, S. Kokubun, T. Mukai, T. Nagai, and A. A. Petrukovich (1999a), Substorm dipolarization and recovery, *J. Geophys. Res.*, *104*, 24,995–25,000, doi:10.1029/1999JA900282.

Baumjohann, W., R. A. Treumann, E. Georgescu, G. Haerendel, K.-H. Fornacon, and U. Auster (1999b), Waveform and packet structure of lion roars, *Ann. Geophys.*, *17*, 1528–1534, doi:10.1007/s00585-999-1528-9.

Baumjohann, W., E. Georgescu, K.-H. Fornacon, H. U. Auster, R. A. Treumann, and G. Haerendel (2000), Magnetospheric lion roars, *Ann. Geophys.*, *18*, 406–410, doi:10.1007/s00585-000-0406-2.

Birn, J., and M. Hesse (2005), Energy release and conversion by reconnection in the magnetotail, *Ann. Geophys.*, *23*, 3365–3373, doi:10.5194/angeo-23-3365-2005.

Birn, J., M. Hesse, G. Haerendel, W. Baumjohann, and K. Shiokawa (1999), Flow braking and the substorm current wedge, *J. Geophys. Res.*, *104*, 19,895–19,904, doi:10.1029/1999JA900173.

Birn, J., J. Raeder, Y. Wang, R. Wolf, and M. Hesse (2004), On the propagation of bubbles in the geomagnetic tail, *Ann. Geophys.*, *22*, 1773–1786.

Birn, J., R. Nakamura, E. V. Panov, and M. Hesse (2011), Bursty bulk flows and dipolarization in MHD simulations of magnetotail reconnection, *J. Geophys. Res.*, *116*, doi:10.1029/2010JA016083.

Borodkova, N. L., A. G. Yahnin, K. Liou, J.-A. Sauvaud, A. O. Fedorov, V. N. Lutsenko, M. N. Nozdrachev, and A. A. Lyubchich (2002), Plasma sheet fast flows and auroral dynamics during substorm: A case study, *Ann. Geophys.*, *20*, 341–347, doi:10.5194/angeo-20-341-2002.

Bortnik, J., R. M. Thorne, and U. S. Inan (2008), Nonlinear interaction of energetic electrons with large amplitude chorus, *Geophys. Res. Lett.*, *35*, L21102, doi:10.1029/2008GL035500.

Boström, R. (1964), A model of the auroral electrojects, *J. Geophys. Res.*, *69*, 4983–4999, doi:10.1029/JZ069i023p04983.

Cattell, C., et al. (2008), Discovery of very large amplitude whistler-mode waves in Earth's radiation belts, *Geophys. Res. Lett.*, *35*, L01105, doi:10.1029/2007GL032009.

Chen, C. X., and R. A. Wolf (1999), Theory of thin-filament motion in Earth's magnetotail and its application to bursty bulk flows, *J. Geophys. Res.*, *104*, 14,613–14,626, doi:10.1029/1999JA900005.

Deng, X., M. Ashour-Abdalla, M. Zhou, R. Walker, M. El-Alaoui, V. Angelopoulos, R. E. Ergun, and D. Schriver (2010), Wave and particle characteristics of earthward electron injections associated with dipolarization fronts, *J. Geophys. Res.*, *115*, A09225, doi:10.1029/2009JA015107.

Elphinstone, R. D., J. S. Murphree, and L. L. Cogger (1996), What is a global auroral substorm? *Rev. Geophys.*, *34*, 169–232, doi:10.1029/96RG00483.

Elphinstone, R. D., et al. (1995), Observations in the vicinity of substorm onset: Implications for the substrom process, *J. Geophys. Res.*, *100*, 7937–7969, doi:10.1029/94JA02938.

Erickson, G. M., and R. A. Wolf (1980), Is steady convection possible in the earth's magnetotail, *Geophys. Res. Lett.*, *7*, 897–900, doi:10.1029/GL007i011p00897.

Frey, H. U., et al. (2010), Small and meso-scale properties of a substorm onset auroral arc, *J. Geophys. Res.*, *115*, doi:10.1029/2010JA015537.

Fu, H. S., Y. V. Khotyaintsev, M. André, and A. Vaivads (2011), Fermi and betatron acceleration of suprathermal electrons behind dipolarization fronts, *Geophys. Res. Lett.*, *38*, L16104, doi:10.1029/2011GL048528.

Ginzburg, V. L, and A. A. Rukhadze (1975), *Waves in Magnetoactive Plasma,* 2nd rev. ed., Nauka, Moscow, Russia.

Glauert, S. A., and R. B. Horne (2005), Calculation of pitch angle and energy diffusion coefficients with the PADIE code, *J. Geophys. Res.*, *110*, A04206, doi:10.1029/2004JA010851.

Haerendel, G. (1992), Disruption, ballooning or auroral avalanche-on the cause of substorms, *in Proceedings of the First International Conference on Substorms, Kiruna, Sweden, 23-27 March 1992, ESA Spec. Publ., SP-337*, 417–420.

Haerendel, G. (2010), Equatorward moving arcs and substorm onset, *J. Geophys. Res.*, *115*, A07212, doi:10.1029/2009JA015117.

Hayakawa, H., A. Nishida, Jr. E. W. Hones, and S. J. Bame (1982), Statistical characteristics of plasma flow in the magnetotail, *J. Geophys. Res.*, *87*, 277–283, doi:10.1029/JA087iA01p00277.

Henderson, M. G., G. D. Reeves, and J. S. Murphree (1998), Are north-south aligned auroral structures an ionospheric manifestation of bursty bulk flows? *Geophys. Res. Lett.*, *25*, 3737–3740, doi:10.1029/98GL02692.

Huang, S. Y., M. Zhou, X. H. Deng, Z. G. Yuan, Y. Pang, Q. Wei, W. Su, H. M. Li, and Q. Q. Wang (2012), Kinetic structure and wave properties associated with sharp dipolarization front observed by Cluster, *Ann. Geophys.*, *30*, 97–107, doi:10.5194/angeo-30-97-2012.

Keiling, A., K. Shiokawa, V. Uritsky, V. Sergeev, E. Zesta, L. Kepko, and N. Østgaard (2012), Auroral signatures of the dynamic plasma sheet, in *Auroral Phenomenology and Magnetospheric Processes: Earth and Other Planets, Geophys. Monogr. Ser.,* vol. 197, edited by A. Keiling et al., pp. 317–335, AGU, Washington, D. C., doi:10.1029/2012GM001231.

Keiling, A., et al. (2009a), THEMIS ground-space observations during the development of auroral spirals, *Ann. Geophys.*, *27*, 4317–4332, doi:10.5194/angeo-27-4317-2009.

Keiling, A., et al. (2009b), Substorm current wedge driven by plasma flow vortices THEMIS observations, *J. Geophys. Res.*, *114*, A00C22, doi:10.1029/2009JA014114.

Kennel, C. F., and H. E. Petschek (1966), Limit on stably trapped particle fluxes, *J. Geophys. Res.*, *71*, 1.

Kepko, L., M. G. Kivelson, R. L. McPherron, and H. E. Spence (2004), Relative timing of substorm onset phenomena, *J. Geophys. Res.*, *109*, A04203, doi:10.1029/2003JA010285.

Kepko, L., E. Spanswick, V. Angelopoulos, E. Donovan, J. McFadden, K.-H. Glassmeier, J. Raeder, and H. J. Singer (2009), Equatorward moving auroral signatures of a flow burst observed prior to auroral onset, *Geophys. Res. Lett.*, *36*, doi:10.1029/2009GL041476.

Khotyaintsev, Y. V., C. M. Cully, A. Vaivads, M. André, and C. J. Owen (2011), Plasma jet braking: energy dissipation and nonadiabatic electrons, *Phys. Rev. Lett.*, *106*(16), 165001, doi:10.1103/PhysRevLett.106.165001.

Le Contel, O., et al. (2009), Quasi-parallel whistler mode waves observed by THEMIS during near-earth dipolarizations, *Ann. Geophys.*, *27*, 2259–2275, doi:10.5194/angeo-27-2259-2009.

Liang, J., E. Spanswick, M. J. Nicolls, E. F. Donovan, D. Lummerzheim, and W. W. Liu (2011), Multi-instrument observations of soft electron precipitation and its association with magnetospheric flows, *J. Geophys. Res.*, *116*, A06201, doi:10.1029/2010JA015867.

Liang, J., B. Ni, C. M. Cully, E. F. Donovan, R. M. Thorne, and V. Angelopoulos (2012), Electromagnetic ELF wave intensification associated with fast earthward flows in mid-tail plasma sheet, *Ann. Geophys.*, *30*, 467–488, doi:10.5194/angeo-30-467-2012.

Lui, A. T. Y., E. Spanswick, E. F. Donovan, J. Liang, W. W. Liu, O. Le Contel, and Q.-G. Zong (2010), A transient narrow poleward extrusion from the diffuse aurora and the concurrent magnetotail activity, *J. Geophys, Res.*, *115*, A10210, doi:10.1029/2010JA015449.

Lyons, L. R. (1974), Pitch angle and energy diffusion coefficients from resonant interactions with ion-cyclotron and whistler waves, *J. Plasma Phys.*, *12*, 417–432, doi:10.1017/S002237780002537X.

Lyons, L. R., T. Nagai, G. T. Blanchard, J. C. Samson, T. Yamamoto, T. Mukai, A. Nishida, and S. Kokobun (1999), Association between Geotail plasma flows and auroral poleward boundary intensifications observed by CANOPUS photometers, *J. Geophys. Res.*, *104*, 4485–4500, doi:10.1029/1998JA900140.

Lyons, L. R., Y. Nishimura, X. Xing, A. Runov, V. Angelopoulos, E. Donovan, and T. Kikuchi (2012), Coupling of dipolarization front flow bursts to substorm expansion phase phenomena within the magnetosphere and ionosphere, *J. Geophys. Res.*, *117*, A02212, doi:10.1029/2011JA017265.

Lyons, L. R., et al. (2011), Possible connection of polar cap flows to pre- and post-substorm onset PBIs and streamers, *J. Geophys. Res.*, *116*, A12225, doi:10.1029/2011JA016850.

McFadden, J. P., C. W. Carlson, D. Larson, M. Ludlam, R. Abiad, B. Elliott, P. Turin, M. Marckwordt, and V. Angelopoulos (2008), The THEMIS ESA plasma instrument and in-flight calibration, *Space Sci. Rev.*, *141*, 277–302, doi:10.1007/s11214-008-9440-2.

Mende, S. B., S. E. Harris, H. U. Frey, V. Angelopoulos, C. T. Russell, E. Donovan, B. Jackel, M. Greffen, and L. M. Peticolas (2008), The THEMIS array of ground-based observatories for the study of auroral substorms, *Space Sci. Rev.*, *141*, 357–387, doi:10.1007/s11214-008-9380-X.

Mourenas, D., A. Artemyev, O. Agapitov, and V. Krasnoselskikh (2012a), Acceleration of radiation belts electrons by oblique chorus waves, *J. Geophys. Res.*, *117*, A10212, doi:10.1029/2012JA018041.

Mourenas, D., A. V. Artemyev, J.-F. Ripoll, O. V. Agapitov, and V. V. Krasnoselskikh (2012b), Timescales for electron quasi-linear diffusion by parallel and oblique lower-band chorus waves, *J. Geophys. Res.*, *117*, A06,234, doi:10.1029/2012JA017717.

Nakamura, R., T. Oguti, T. Yamamoto, and S. Kokubun (1993), Equatorward and poleward expansion of the auroras during auroral substorms, *J. Geophys. Res.*, *98*, 5743–5759, doi:10.1029/92JA02230.

Nakamura, R., W. Baumjohann, M. Brittnacher, V. A. Sergeev, M. Kubyshkina, T. Mukai, and K. Liou (2001a), Flow bursts and auroral activations: Onset timing and foot point location, *J. Geophys. Res.*, *106*, 10,777–10,790, doi:10.1029/2000JA000249.

Nakamura, R., W. Baumjohann, R. Schödel, M. Brittnacher, V. A. Sergeev, M. Kubyshkina, T. Mukai, and K. Liou (2001b), Earthward flow bursts, auroral streamers, and small expansions, *J. Geophys. Res.*, *106*, 10,791–10,802, doi:10.1029/2000JA000306.

Nakamura, R., et al. (2004), Spatial scale of high-speed flows in the plasma sheet observed by Cluster, *Geophys. Res. Lett.*, *31*, L09804, doi:10.1029/2004GL019558.

Ni, B., R. M. Thorne, R. B. Horne, N. P. Meredith, Y. Y. Shprits, L. Chen, and W. Li (2011a), Resonant scattering of plasma sheet electrons leading to diffuse auroral precipitation: 1. Evaluation for electrostatic electron cyclotron harmonic waves, *J. Geophys. Res.*, *116*, A04218, doi:10.1029/2010JA016232.

Ni, B., R. M. Thorne, N. P. Meredith, Y. Y. Shprits, and R. B. Horne (2011b), Diffuse auroral scattering by whistler mode chorus waves: Dependence on wave normal angle distribution, *J. Geophys. Res.*, *116*, A10207, doi:10.1029/2011JA016517.

Nishimura, Y., et al. (2010), Identifying the driver of pulsating Aurora, *Science*, *330*, 81–, doi:10.1126/science.1193186.

Ohtani, S., Y. Miyashita, H. Singer, and T. Mukai (2009), Tailward flows with positive B_Z in the near-Earth plasma sheet, *J. Geophys. Res.*, *114*, A06218, doi:10.1029/2009JA014159.

Omura, Y., and Q. Zhao (2012), Nonlinear pitch angle scattering of relativistic electrons by EMIC waves in the inner magnetosphere, *J. Geophys. Res.*, *117*, A08227, doi:10.1029/2012JA017943.

Panov, E. V., V. A. Sergeev, P. L. Pritchett, F. V. Coroniti, R. Nakamura, W. Baumjohann, V. Angelopoulos, H. U. Auster, and J. P. McFadden (2012a), Observations of kinetic ballooning/interchange instability signatures in the magnetotail, *Geophys. Res. Lett.*, *39*, L08110, doi:10.1029/2012GL051668.

Panov, E. V., et al. (2010a), Plasma sheet thickness during a bursty bulk flow reversal, *J. Geophys. Res.*, *115*, A05213, doi:10.1029/2009JA014743.

Panov, E. V., et al. (2010b), Multiple overshoot and rebound of a bursty bulk flow, *Geophys. Res. Lett.*, *37*, L08103, doi:10.1029/2009GL041971.

Panov, E. V., et al. (2013b), Ionospheric response to oscillatory flow braking in the magnetotail, *J. Geophys. Res. Space Physics*, *118*, doi:10.1002/jgra.50190.

Paschmann, G., S. Haaland, and R. Treumann (2002), Auroral plasma physics, *Space Sci. Rev.*, *103*, 1–477, doi:10.1023/A:1023030716698.

Pontius, D. H., Jr., and R. A. Wolf (1990), Transient flux tubes in the terrestrial magnetosphere, *Geophys. Res. Lett.*, *17*, 49–52, doi:10.1029/GL017i001p00049.

Pritchett, P. L., and F. V. Coroniti (2010), A kinetic ballooning/interchange instability in the magnetotail, *J. Geophys. Res.*, *115*, A06301, doi:10.1029/2009JA014752.

Roux, A., O. Le Contel, C. Coillot, A. Bouabdellah, B. de La Porte, D. Alison, S. Ruocco, and M. C. Vassal (2008), The search coil magnetometer for THEMIS, *Space Sci. Rev.*, *141*, 265–275, doi:10.1007/s11214-008-9455-8.

Semenov, V. S., and V. V. Lebedeva (1991), Model problem of the reconnection of fine magnetic flux tubes in the cusp region, *Geomag. Aeron.*, *31*, 974–981.

Sergeev, V., K. Liou, P. Newell, S. Ohtani, M. Hairston, and F. Rich (2004), Auroral streamers: Characteristics of associated precipitation, convection and field-aligned currents, *Ann. Geophys.*, *22*, 537–548, doi:10.5194/angeo-22-537-2004.

Sergeev, V. A., V. Angelopoulos, J. T. Gosling, C. A. Cattell, and C. T. Russell (1996), Detection of localized, plasma-depleted flux tubes or bubbles in the midtail plasma sheet, *J. Geophys. Res.*, *101*, 10,817–10,826, doi:10.1029/96JA00460.

Sergeev, V. A., K. Liou, C.-I. Meng, P. T. Newell, M. Brittnacher, G. Parks, and G. D. Reeves (1999), Development of auroral streamers in association with localized impulsive injections to the inner magnetotail, *Geophys. Res. Lett.*, *26*, 417–420, doi:10.1029/1998GL900311.

Sergeev, V. A., M. V. Kubyshkina, K. Liou, P. T. Newell, G. Parks, R. Nakamura, and T. Mukai (2001), Substorm and convection bay compared: Auroral and magnetotail dynamics during convection bay, *J. Geophys. Res.*, *106*, 18,843–18,856, doi:10.1029/2000JA900087.

Sergeev, V. A., et al. (2000), Multiple-spacecraft observation of a narrow transient plasma jet in the Earth's plasma sheet, *Geophys. Res. Lett.*, *27*, 851–854, doi:10.1029/1999GL010729.

Shiokawa, K., W. Baumjohann, and G. Haerendel (1997), Braking of high-speed flows in the near-Earth tail, *Geophys. Res. Lett.*, *24*, 1179–1182, doi:10.1029/97GL01062.

Shiokawa, K., G. Haerendel, and W. Baumjohann (1998a), Azimuthal pressure gradient as driving force of substorm currents, *Geophys. Res. Lett.*, *25*, 959–962, doi:10.1029/98GL00540.

Shiokawa, K., et al. (1998b), High-speed ion flow, substorm current wedge, and multiple Pi 2 pulsations, *J. Geophys. Res.*, *103*, 4491–4508, doi:10.1029/97JA01680.

Shklyar, D., and H. Matsumoto (2009), Oblique whistler-mode waves in the inhomogeneous magnetospheric plasma: Resonant interactions with energetic charged particles, *Surveys Geophys.*, *30*, 55–104, doi:10.1007/s10712-009-9061-7.

Solovev, V. V., and D. R. Shkliar (1986), Particle heating by a low-amplitude wave in an inhomogeneous magnetoplasma, *Sov. Phys. JETP*, *63*, 272–277.

Summers, D., R. M. Thorne, and F. Xiao (1998), Relativistic theory of wave-particle resonant diffusion with application to electron acceleration in the magnetosphere, *J. Geophys. Res.*, *103*, 20,487–20,500, doi:10.1029/98JA01740.

Thorne, R. M., B. Ni, X. Tao, R. B. Horne, and N. P. Meredith (2010), Scattering by chorus waves as the dominant cause of diffuse auroral precipitation, *Nature*, *467*, 943–946, doi:10.1038/nature09467.

Trakhtengerts, V. Y. (1966), Stationary states of the Earth's outer radiation zone, *Geomag. Aeron.*, *6*, 827–836.

Untiedt, J., and W. Baumjohann (1993), Studies of polar current systems using the IMS Scandinavian magnetometer array, *Space Sci. Rev.*, *63*, 245–390, doi:10.1007/BF00750770.

Uritsky, V. M., J. Liang, E. Donovan, E. Spanswick, D. Knudsen, W. Liu, J. Bonnell, and K. H. Glassmeier (2009), Longitudinally propagating arc wave in the pre-onset optical aurora, *Geophys. Res. Lett.*, *36*, L21103, doi:10.1029/2009GL040777.

Vedenov, A. A., and R. Z. Sagdeev (1961), Some properties of a plasma with an anisotropic ion velocity distribution in a magnetic field, in *Plasma Physics and the Problem of Controlled Thermonuclear Reactions,* vol. 3, edited by M. A. Leontovich, p. 332, Pergamon Press, Hardback.

Wei, X. H., et al. (2007), Cluster observations of waves in the whistler frequency range associated with magnetic reconnection in the Earth's magnetotail, *J. Geophys. Res.*, *112*, A10225, doi:10.1029/2006JA011771.

Wolf, R. A., C. X. Chen, and F. R. Toffoletto (2012a), Thin filament simulations for Earth's plasma sheet: Interchange oscillations, *J. Geophys. Res.*, *117*, A02215, doi:10.1029/2011JA016971.

Wolf, R. A., C. X. Chen, and F. R. Toffoletto (2012b), Thin filament simulations for Earth's plasma sheet: Tests of validity of the quasi-static convection approximation, *J. Geophys. Res.*, *117*, A02216, doi:10.1029/2011JA016972.

Zesta, E., E. Donovan, L. Lyons, G. Enno, J. S. Murphree, and L. Cogger (2002), Two-dimensional structure of auroral poleward boundary intensifications, *J. Geophys. Res.*, *107*, 1350, doi:10.1029/2001JA000260.